Jamming Skins that Control System Rigidity from the Surface

Dylan S. Shah, Ellen J. Yang, Michelle C. Yuen, Evelyn C. Huang, and Rebecca Kramer-Bottiglio*

Numerous animals adapt their stiffness during natural motions to increase efficiency or environmental adaptability. For example, octopuses stiffen their tentacles to increase efficiency during reaching, and several species adjust their leg stiffness to maintain stability when running across varied terrain. Inspired by nature, variable-stiffness machines can switch between rigid and soft states. However, existing variable-stiffness systems are usually purpose-built for a particular application and lack universal adaptability. Here, reconfigurable stiffness-changing skins that can stretch and fold to create 3D structures or attach to the surface of objects to influence their rigidity are presented. These "jamming skins" employ vacuum-powered jamming of interleaved, discrete planar elements, enabling 2D stretchability of the skin in its soft state. Stretching allows jamming skins to be reversibly shaped into load-bearing, functional tools on-demand. Additionally, they can be attached to host structures with complex curvatures, such as robot arms and portions of the human body, to provide support or create a mold. We also show how multiple skins can work together to modify the workspace of a continuum robot by creating instantaneous joints. Jamming skins thus serve as a reconfigurable approach to creating tools and adapting structural rigidity on-demand.

1. Introduction

Biological organisms leverage a wide range of material properties to adapt to their environments: soft, flexible fish swim efficiently through water, while the rigid skeletons of large land mammals allow them to support their body weight. Many animals actively control their stiffness to facilitate motion, such as an elephant grasping with its trunk,[1] octopuses creating virtual joints during reaching motions,[2] and goats adapting their legs as they travel over compliant surfaces.[3] Drawing inspiration from the versatility of these biological systems,[4] engineers have designed "variable stiffness" robots and machines,[5,6] which reversibly switch between rigid and soft states, trading load-bearing capabilities for flexibility. Approaches to creating

variable stiffness mechanisms include stimuli-responsive materials,[7–9] system-level antagonistic control,[10–12] and pressure-induced material interlocking or "jamming."[13,14] In this study, we explore a new form of material jamming through adaptive, planar skins that can reversibly stretch in two dimensions to be sculpted into complex 3D shapes, and rigidly maintain that shape to serve as tools and exoskeletons for soft objects.

Material jamming uses pressure to control the interaction between disconnected pieces of inextensible material (either granular,[15–19] planar,[20] or fibrous[21]) enabling a transition between soft and rigid states. For example, in atmospheric conditions, particles such as sand or coffee easily slide over each other in a fluid-like state, but when pressed together, the grains pack tightly and resist shear like a solid.[22] Seeking thin variable-stiffness solutions, researchers have introduced "layer jamming" systems where 2D layers of inextensible material, such as sheets of paper[14] or polyethylene terephthalate (PET),[23] are pressed from a flexible state into a rigid state by surrounding the sheets in a compliant membrane and applying a vacuum. Unobtrusive layer jamming systems have been proven in a variety of applications, including compliance control of continuum robotic segments,[24,25] variable-stiffness continuum manipulators,[5,24,25] selectively compliant grippers,[14,23] and variable-stiffness furniture.[26] However, these jamming approaches either could not stretch,[20] or could only stretch in one direction,[23,27,28] so they are unable to access complex shapes with compound curvatures, limiting their versatility.

Achieving 2D stretchability is a strict requirement for creating a universal, shape-locking skin. Gauss' Theorema Egregium states that inextensible sheets must experience plastic deformation when bent from their initial flat shape (with uniformly zero Gauss curvature), into more complicated shapes with nonzero Gauss curvature (e.g., spheres, hyperboloids).[29] In other words, to reversibly adapt to 3D shapes with compound curvatures, a surface needs to be stretchable along two orthogonal directions. Traditional layer jamming systems, only able to stretch along one dimension, have exclusively been able to accommodate curvature about a single axis, practically limiting them to shapes such as cylinders or sequences of

D. S. Shah, E. J. Yang, Dr. M. C. Yuen, E. C. Huang,
Prof. R. Kramer-Bottiglio
School of Engineering & Applied Science
Yale University
17 Hillhouse Avenue, New Haven, CT 06520, USA
E-mail: rebecca.kramer@yale.edu

The ORCID identification number(s) for the author(s) of this article can be found under https://doi.org/10.1002/adfm.202006915.

**ADVANCED
SCIENCE NEWS**
www.advancedsciencenews.com

**ADVANCED
FUNCTIONAL
MATERIALS**
www.afm-journal.de

discrete folds. Two notable recent approaches have attempted to overcome these limitations. First, researchers interleaved hoops and helices of inextensible material to create sheaths for bendable continuum arms with constant cross-section.[24,25] Another proposed approach involves building jammable interfaces from piled stretchable fabrics.[30] While promising, these prior jamming approaches were tailored to specific applications. For example, the manipulators[24,25] could not be repurposed into jammable interfaces[30] or jamming furniture,[26] and vice versa.

In this work, we introduce thin, reconfigurable "jamming skins" that can stretch in two dimensions to unobtrusively accommodate numerous shapes with complex surface curvatures. These jamming skins can be fabricated using a generalizable and scalable manufacturing method to accommodate a wide range of design constraints. We show these skins accomplishing a wide range of tasks, including adjusting the trajectory of a soft robot arm to increase its workspace, serving as a reconfigurable wrist brace, and building complex structures on-demand (**Figure 1**). After use in one application, the skins can be removed and applied to another host body, or be repurposed to create a standalone tool. Their activation mechanism is fast and simple, requiring only application and removal of vacuum pressure to trigger stiffness change. 2D stretchable jamming skins have a wide range of applications, from providing unobtrusive physical support for users with joint instabilities, to serving as a reconfigurable tool for use in constrained and/or resource-limited environments.
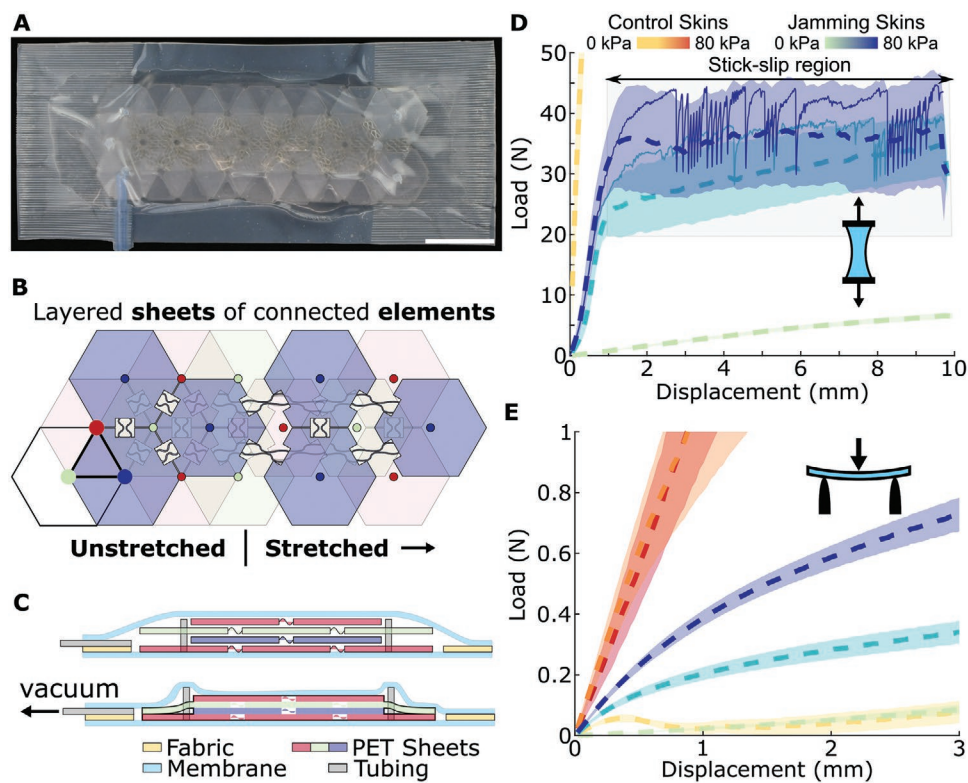
2. Results

Jamming skins are composed of a sealed, stretchable membrane containing layers of small overlapping sheets of intrinsically inextensible material (jamming elements), linked to prevent de-interleaving of layers (**Figure 2A–C**). While at atmospheric pressure, elements can slide over each other, enabling global stretchability; under vacuum, the membrane presses the elements together and inter-layer friction prevents further sliding, making the skin stiff and inextensible (Movie S1, Supporting Information). A typical skin could transition from stretchable to fully jammed (−80 kPa) in under 4 s using a vacuum pump. Several design parameters can be adjusted to fit application requirements, if desired. For example, varying membrane and jamming materials results in different stiffening characteristics when activated,[16,23,27] and increasing the number of layers (n) makes the skin thicker but improves the stiffening ratio (scaling with n^2,[14] discussed in Suopporting Information). Here, we specifically demonstrate jamming elements cut into hexagonal shapes from a single sheet of inextensible polyethylene teraphthalate (PET) using a laser cutter, with 2D spring-like serpentine links[31] connecting each element to enable global stretchability (Figure 2A,B). The serpentine links prevent the jamming elements from sliding around inside of a stretchable silicone membrane, ensuring maximum interleaving of jamming elements throughout multiple stretching and jamming cycles. Additional jamming skins, including a springless design, were manufactured and compared to this main embodiment (Figures S1 and S2, supporting Information). However, we found that this main embodiment (hexagonal elements with springs, as shown in Figure 2) had the highest stiffness ratio while also being significantly less labor-intensive than the springless designs.

Jamming skins can actively change their in-plane (tensile) and out-of plane (bending) stiffness, allowing them to adjust an enveloped body's system dynamics from the surface. To achieve stiffness changes, layer jamming relies on inter-layer
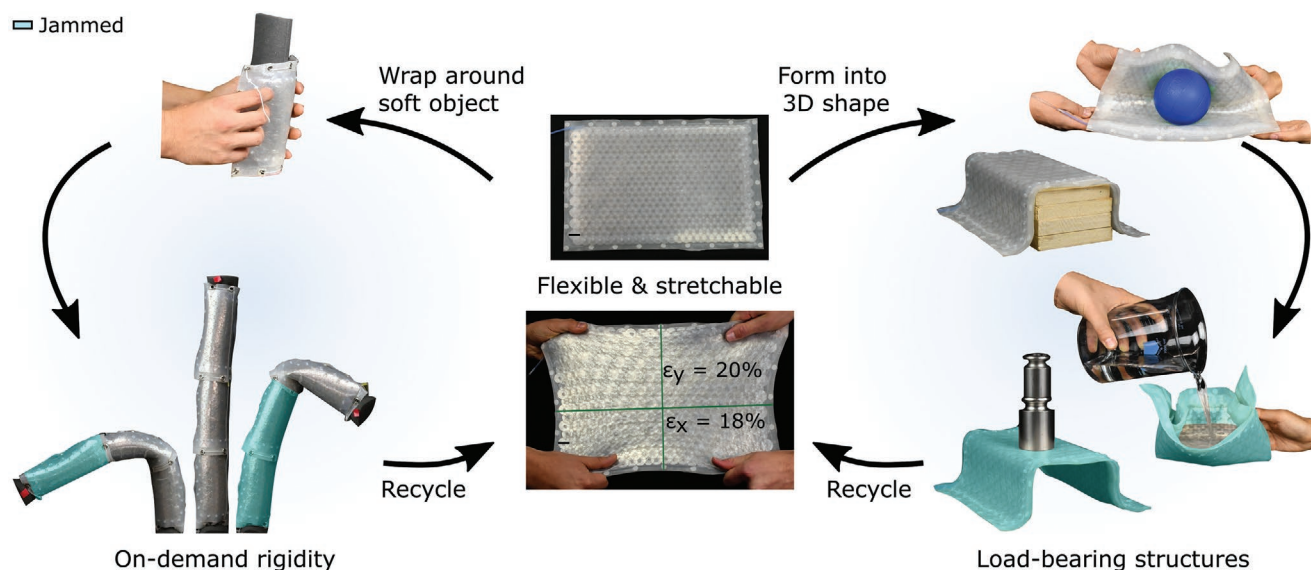
Figure 1. Jamming skins can be applied to the surface of deformable objects to provide support, or be reconfigured to create structures and tools on-demand. Upon application of a vacuum, the skins transition from flexible and stretchable sheets (no added shading) to stiff surfaces (cyan). Applications shown in the bottom row, from left to right: continuum manipulator with on-demand joints, reconfigurable table, sculptable reservoir for holding liquids.

2006915 (2 of 8)

**ADVANCED
SCIENCE NEWS**
www.advancedsciencenews.com

**ADVANCED
FUNCTIONAL
MATERIALS**
www.afm-journal.de

Figure 2. Jamming skins consist of a stretchable membrane and interleaved inextensible elements. A) Top view of a jamming skin. Scale bar is 2.5 cm. B) PET is laser cut to create numerous jamming elements (here, hexagons) that are centered around regularly spaced nodes (denoted by colored dots). Elements within a single layer are connected by serpentine springs of PET. Different colors indicate the three unique layer designs which are stacked and staggered relative to each other. C) Principle of operation, showing the unjammed state (top) and the jammed, inextensible state (bottom). D) Jamming skins have increasing in-plane stiffness at increasing vacuum pressure. The control skin, with homogeneous rectangles of PET, is inextensible and consistently ripped during testing. Solid lines are representative curves. E) Bending stiffness increases with increasing applied membrane pressure. (D,E) Shaded regions represent 1 standard deviation, dashed lines represent the mean.

friction to prevent elements from slipping in the presence of shear stress. Coulomb friction models have been used as first-order models to design traditional layer jamming systems under both tensile and bending loading conditions,[14,21,24,25,27,32] and can be adopted to generate performance predictions and design goals for our stretchable jamming skins. For example, Coulomb models predict that the maximum tensile loading force prior to slip $F(\mu, A, P)$ is linear for all independent variables, yielding $F \propto \mu*A*P$, where μ is the inter-layer friction coefficient, A is the total area of overlap between elements in each cross-section, and P denotes the applied vacuum pressure (derivation presented in Supporting Information). A similar prediction can be made for the bending case, as discussed in the Supporting Information. Thus, for a given jamming skin design, large changes in maximum loading can be quickly attained by increasing the vacuum pressure. Regardless of loading condition, to maximize jammed stiffness while minimizing thickness (which also minimizes the unjammed stiffness and the attainable radius of curvature), it is desirable to maximize the overlap area.

We developed a generalizable procedure to design each layer of PET and attain maximum element overlap, which we applied to create the hexagonal element patterns shown throughout this paper. First, we distributed the jamming elements' centers at nodes defined by the vertices of a simple, patternable base shape (e.g., a triangle, square or hexagon) tiled throughout the jamming area. For our demonstrations, we used a triangular tiling because of its simplicity and dense packing as shown in Figure 2B. One vertex of each tiled triangle was assigned to each of three unique layers, and elements in each layer were centered at each vertex (node) (shown by the different colored nodes in Figure 2B). This enabled neighboring elements, situated in different layers, to slide relative to each other (Figure 2B,C), while maintaining surface-to-surface contact such that they would interlock when the skin was activated.

Once the nodes were assigned to their appropriate layers, we could uniquely determine the shape and size of each PET jamming element with the maximum overlap between jamming elements. First, we computed the Delaunay triangulation[33] for each layer design. Then, we connected the Delaunay nodes to create Voronoi diagrams that evenly divided the space between nodes, without producing gaps. This resulted in zero wasted material (except for slots required to make the springs) and maximized jamming element overlap, thereby increasing the attainable stiffness change. The triangular tiling used in our demonstration generated hexagonal elements, as shown in Figure 2B. Delaunay triangulations can be efficiently calculated for arbitrary node distributions,[33] enabling rapid design of jamming skins that require an irregular node spacing due to other design constraints. Once the design of the three layers was set, the skins were manufactured by stacking multiple

layers of each design ($n = 12$ total layers), and sealing the stack inside a stretchable silicone membrane.

To quantify the performance of the manufactured jamming skins, we measured their mechanical response in tension and bending, while varying the applied vacuum pressure (Figure 2D,E). We also compared the stretchable skins to a control set of identically sized skins containing homogeneous rectangular PET sheets (Figure 2D,E and Figure S3, Supporting Information), representing traditional layer jamming systems (inextensible layers in flexible membranes[14,20,34]). All of the control skins ripped after stretching more than a few percent strain, which prevented us from performing any meaningful tensile tests at any vacuum pressures other than ambient conditions. In contrast, the jamming skins could repeatedly stretch to ≈20% strain while unjammed (average stiffness of 0.67 ± 0.05 N m^{-1} standard deviation), and were relatively inextensible while jammed at -80 kPa (31.05 ± 4.97 N m^{-1}), resulting in a jamming ratio of 47. As expected, the unjammed force–displacement behavior was roughly linear throughout the test, because the silicone membrane and PET springs were being freely stretched. While jammed, the tensile response was linear at low strains, but after the tensile load exceeded the maximum friction force and initiated slip, the skins exhibited an oscillatory stick–slip behavior at their PET interfaces (Figure 2D, solid lines). By increasing the pressure from 40 to 80 kPa, the force at slip increased from 25.3 ± 5.0 to 38.1 ± 8.5 N, an increase of 51%, confirming that slip points can be tuned by modulating pressure (Figure S4, Supporting Information). Additionally, we find that pre-slip tensile stiffness is relatively independent of pressure, as predicted by theory (Figure 2D and Supporting Information).

In contrast to the tensile loading condition, during bending, jamming skins exhibit multiple slip points rather than a single slip point (Figure 2E and Supporting Information). This results in multi-linear (as opposed to bilinear) curves with numerous break points that depend on pressure. When coupled with natural inhomogeneities and slight irregularities in surface topography during jamming, the force–displacement curves during bending often exhibited a smoother response. By varying the pressure, users can smoothly tune these slip points and adjust the perceived stiffness.

Although the jamming skins had a lower bending stiffness than the control skins in the jammed state, they were significantly more flexible when unjammed (Figure 2E and Figure S4, Supporting Information). This behavior is primarily a consequence of the stress relief provided by the gaps between elements. As a result, the jamming skins' mean stiffness ratio between the jammed and unjammed states (16.6) was higher than the control skins' (7.9). In summary, the results presented here collectively demonstrate that jamming skins can easily stretch and bend while unjammed, then reversibly switch to an inextensible and inflexible state.

3. Applications

The universal adaptability enabled by the 2D stretchability of jamming skins, along with their rapid state switching, makes them useful in many situations. In this work, we demonstrate them as reconfigurable multitools, load-bearing platforms,

and contour-matching casts. After acquiring one load-bearing shape, the skins can be reconfigured into other shapes to serve different purposes, without requiring modification of the host structures or target shapes. The skins' elasticity and built-in fabric snaps allow them to stretch around a surface and maintain sufficient contact to provide support.

The simplest form of shape locking can be achieved by manually bending jamming skins into a desired shape. For example, a 290 g jamming skin was rolled into a cylinder and, upon activation, the skin stiffened to become load bearing, supporting over 1.5 kg (**Figure 3**A and Movie S2, Supporting Information). Additionally, exploiting the watertight silicone membrane, a skin was formed into a concave shape (nonzero Gauss curvature) and used as a temporary liquid-holding vessel (Figure 1 and Movie S5, Supporting Information). The same skin was reconfigured into numerous other functional shapes including a shovel, a shelter for delicate objects, a book stand, a ramp for robots to ascend, a cup for holding water, stiffening for a manipulator made using robotic skins,[35] and a tool holder (Movie S3 and Figure S5, Supporting Information).

To demonstrate complex 3D contour matching, we placed a jamming skin on top of a variety of objects on a vacuum table. Engaging the vacuum table pulled the skin inward toward the object, prompting the skin to locally stretch and conform to the object's contours. We used this procedure to make the jamming skin match the shape of numerous objects with complex curvatures, including a 3D-printed model of a face, an artificial piece of fruit, and a tape measure (Figure 3B and Movie S4, supporting Information). In particular, the face had a wide range of Gauss curvatures ranging from zero (along the chin) to positive (forehead), to negative (eye sockets), all of which the jamming skin replicated and retained in its final shape. Due to the order-of-magnitude stiffness change experienced by the skins during jamming, the resulting casts could sustain significant external load, as shown in Figure 3B. Since rigidity is proportional to both modulus E and moment of area I, forming the skins into 3D shapes increases the load-bearing capacity relative to the flat configuration (Supporting Information). Thus, by achieving 2D stretchability, jamming skins can reconfigure into complex 3D shapes and gain architectural strength.

We attempted to recreate the shape-locking and structural support capabilities presented here using the control skins (Figure S6, Supporting Information). While the control skins could indeed support loads in several of their jammed configurations, a few deficiencies predicted by the Theorema Egregium and throughout this manuscript were confirmed. The control skins resisted stretching even in their unjammed state, making reconfiguration difficult and making it nearly impossible to accommodate surfaces with nonzero Gauss curvatures. Each control skin ripped after only a few reconfigurations, preventing their long-term usability as a reconfigurable multitool. In order to approximate surfaces with nonzero Gauss curvatures, the control skins had to be folded and creased. This caused permanent plastic deformation of the jamming elements, making them hold their shape even after the vacuum was removed. In contrast, all of the jamming skins used in this manuscript underwent dozens of uses, and have yet to fail during normal use (i.e., without being punctured or over-stretched).
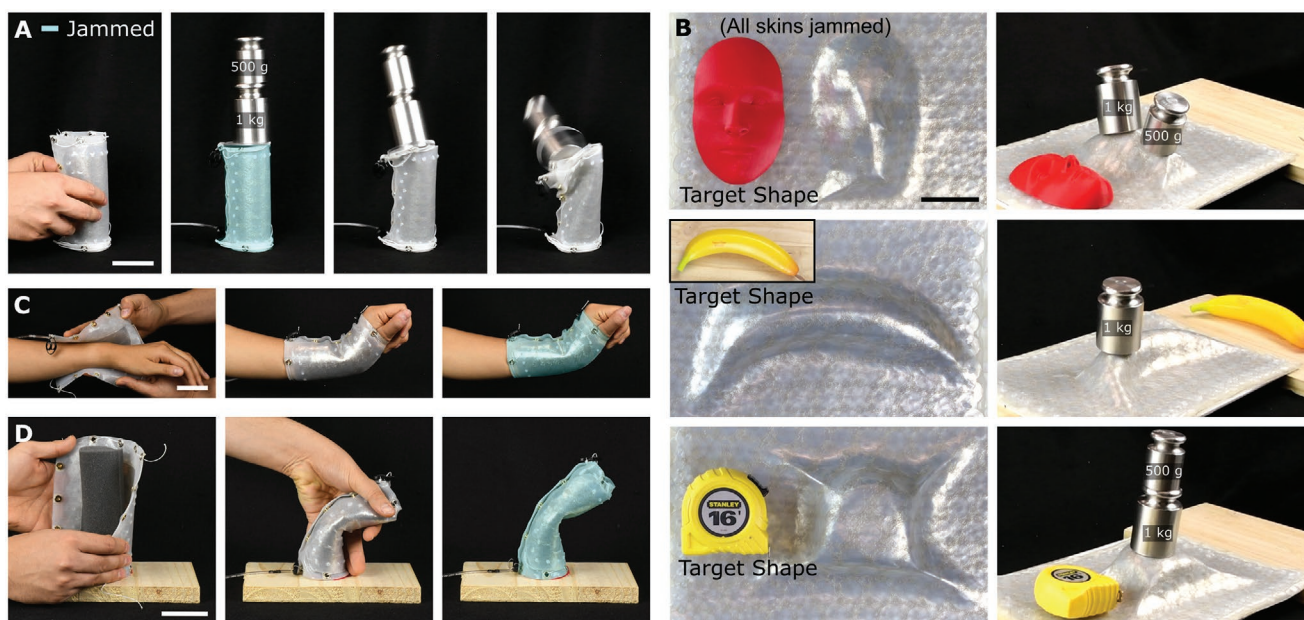
Figure 3. Jamming skins can be reconfigured to form load-bearing 3D shapes or to lend rigidity to soft structures. A) A jamming skin rolled into a rigid cylinder. B) Left column: A single jamming skin matching the shape of a 3D printed face, a banana, and a tape measure. Right column: the skin locked into the same shapes, supporting weights. C) Supporting a user's wrist. D) Locking a foam tube into a bent shape. All scale bars are 5 cm.

When stretched around the surface of objects, jamming skins provide support analogous to an exoskeleton: the rigidity of the relatively thin layer prevents the softer underlying structure from further deforming (Figure 3C,D). For example, the jamming skin provided joint support which could be useful for rehabilitation purposes (Figure 3C and Movie S5, Supporting Information). While unjammed, the skin bends with the user's motion. By varying the pressure, the skin's rigidity could be adjusted to apply varying levels of resistance, or even immobilization of the encased joint. The same jamming skin was applied to a foam tube where it stretched and compressed with the tube, then maintained deformed shapes (Figure 3D and Movie S6, Supporting Information). This jamming skin was also used to create joints on-demand in a continuum manipulator (**Figure 4**), showing the reconfigurability and versatility of an individual skin.

During reaching motions, octopuses generate virtual joints in their tentacles, allowing them to dexterously grab their target.[2] Seeking to emulate this virtual-joint technique, we applied jamming skins to a robotic continuum arm, creating joints on-demand that enabled dynamic adjustment of the operating workspace (Figure 4A). We applied three jamming skins in series along a foam cylinder, overlapping each other by approximately 1 cm. The manipulator was actuated by a string that was tied to an eyelet at the end, routed through the base, and pulled a fixed distance by a mechanical testing machine. Through selective jamming of each skin, we sampled each of the eight possible combinations and obtained representative deformation curves and attainable trajectories. Bending tended to occur at new joints that appeared near the interfaces between two skins (Figure 4B). The eight permutations roughly clustered into four sets, denoted by the four colors in Figure 4. Relative to the reach attained when all skins were unjammed, the manipulator could adjust its trajectory to achieve tighter
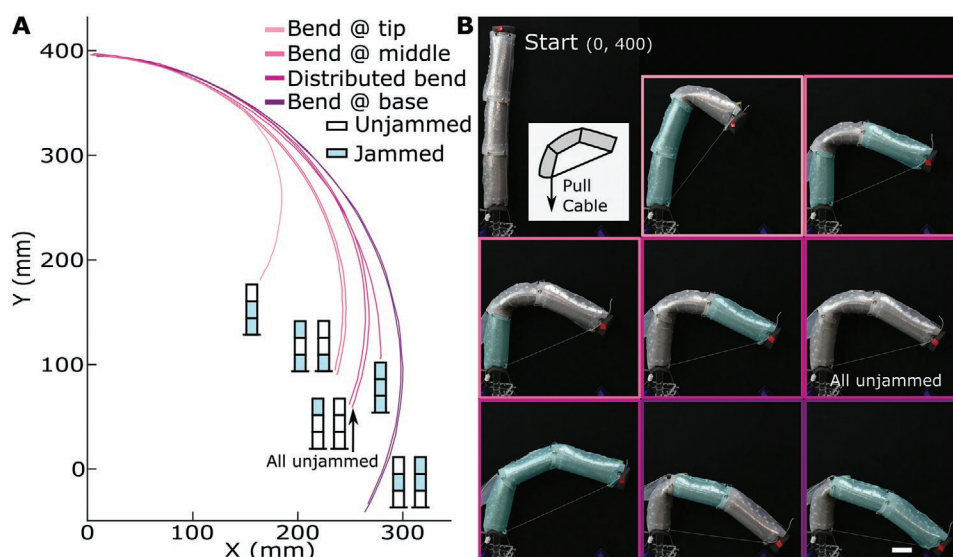
reaches (33% closer to the starting position), as well as wider reaches (27% farther), with the same actuator stroke. Thus, by using the jamming skins to create new joints, a skin-manipulator system could attain multiple workspaces without the need for multiple actuators.

The skins' modularity allows continuum manipulators to be quickly modified, not only in terms of workspace as shown above, but also their materials, design, and construction. To meet the design requirements of a given application, the core of the manipulator could be swapped for another material with different properties. Extra joints could be added by re-configuring or adding jamming skins, new tasks could be completed by adding end-effector tools, or a different actuator could be used (e.g., replace the cable with pneumatic actuators,[36] shape memory alloys[37] or other soft actuators[38]), all without having to re-design the skins.

4. Outlook

This study presents a method for creating thin, elastic skins with controllable in-plane stretchability, and thus, 3D rigidity. By generating space-filling designs that allow interleaved layers of inextensible material to accommodate 2D strains, jamming skins can be flexed and stretched to take on a wide range of 3D forms. Example applications demonstrated in this paper include: reconfigurable load-bearing structures, shape-matching casts, tools that can be quickly re-shaped and re-purposed, human joint support, and on-demand joints for a continuum manipulator.

However, there are a few fundamental limitations which can be addressed through further hardware optimization. During strain, we observed that some of the serpentine springs would snag on neighboring elements and become fully extended

**ADVANCED
SCIENCE NEWS**
www.advancedsciencenews.com

**ADVANCED
FUNCTIONAL
MATERIALS**
www.afm-journal.de

Figure 4. Multiple jamming skins applied to a continuum manipulator to create joints on-demand. A) Depending on the jamming state, the manipulator would bend at a different location, resulting in different end-effector trajectories. Illustrations next to each final end-effector location denote the jamming status of each skin. B) Final configurations. Scale bar is 5 cm. Skins with cyan shading were jammed at a vacuum of ≈85 kPa, while unshaded skins were at atmospheric pressure.

prior to attaining the global strain limit. When this occurred, the springs would pull their connected jamming elements out of the alternating layering pattern, reducing inter-layer friction and weakening the jamming effect. Additionally, neighboring elements on an outermost layer (top, bottom) would occasionally stick to the enclosing membrane, causing a stress concentration and tearing the membrane near their shared edge. To counteract these problems, we simply tuned the spring geometry (longer and narrower springs), and increased the membrane thickness. Each of these solutions comes with a trade-off: longer and narrower springs have less restorative force to return the skins to their initial state, and thicker membranes increase the skins' unjammed stiffness. However, we found that the achieved strain range still enabled our skins to attain a wide range of practical shapes. We suspect that future design optimization and introduction of inextensible materials with higher fracture strains (allowing the springs to stretch farther) will allow the skins to accommodate larger changes in local strain with fewer undesired side-effects.

With higher-fidelity models, jamming skins could be designed to optimally target a set of applications and tasks, while satisfying specific design constraints. At a first approximation, jamming skins can be analyzed using extensions of traditional layer jamming modeling techniques, as discussed in this manuscript. However, the skins' inhomogeneous properties limit the accuracy of predictions generated using such models. While this does not hinder the use of jamming skins in general-purpose applications, it does pose a challenge for designing precise systems that need accurate performance predictions a priori. Additionally, it is unclear how to predict the smallest attainable radius of curvature (κ_{min}) as a function of the skin design. Solving this theoretical problem is important for accurate modeling, since κ_{min} determines the level of detail that jamming skins are able to reproduce when reconfigured or formed to an object. Prior work suggests κ_{min} is on the

same order as the skin thickness,[29] but determining a rigorous model for the minimum bending radius is still an unsolved problem. This type of model will enable design of future jamming skins that optimally balance competing design outcomes, including attainable change in stiffness, shape resolution (i.e., range of attainable shapes), thickness, and maximum strain. Additional inclusion of active, switchable adhesives on the outer membrane could further facilitate shape locking of complex topographies.

The new form of layer jamming presented herein opens up possibilities for designing reconfigurable tools and robots. The hardware is relatively inexpensive, and the skins are quick to activate and reconfigure. We believe that this work will lead to advanced rehabilitative garments and assistive smart clothing, and enable individuals, such as astronauts, to create tools and structures in resource-limited environments. Combined with recent advances in shape-changing robots,[39] sensory skins,[40] stretchable circuits,[41,42] and 3D shape sensing sheets,[43] we envision future robots where the shape and (exo)skeleton of a robot are not fixed, but rather dynamically adaptable to the robot's environment and goals.

5. Experimental Section

Manufacturing: The jamming skins used in this study comprises a silicone membrane (Dragon Skin 10, Smooth-On), and layers of 0.1 mm thick PET that were laser cut (LPKF ProtoLaser U4) to make the jamming elements. Fiber-reinforced silicone[44] was used to connect the membrane seal to the jamming area. For the tension and bending tests, the dimensions of the active jamming area was 130 mm by 45 mm, the width chosen such that two jamming elements could fit side-by-side. Two larger skins based off of this jamming skin design were used for the application-oriented experiments: the 12-layer square membrane (Figures 3A,C,D and Figure 4) had an active jamming area of 130 mm by 130 mm and the larger 20-layer rectangular skin (Figure 3B) had a jamming area of 226 mm by 307 mm (limited by the size of the LPKF

**ADVANCED
SCIENCE NEWS**

www.advancedsciencenews.com

**ADVANCED
FUNCTIONAL
MATERIALS**

www.afm-journal.de

Protolaser U4 used). To provide comparison with prior art, a control set of skins with rectangular (130 × 45 mm) 0.1 mm thick PET in a silicone membrane was also manufactured and tested under tension and bending. Additional designs, mechanical characterization, and manufacturing schematics are presented in the Supporting Information.

Mechanical Characterization Test Procedure: Three specimens of each jamming skin design (designs include the one presented in Figure 2, the control set, and three others discussed in the Supporting Information) were tested on a materials testing machine (Instron 3345) five times each under tension and bending at three pressures (0, 40, and 80 kPa). The tests were performed under quasi-static conditions at 15 mm min^{-1} for tension and 10 mm min^{-1} for bending. Additional details and results regarding characterization are presented in the Supporting Information. Informed signed consent was obtained from the authors that tested the jamming skins in wearable applications, to both participate in the study and to publish any identifiable images.

Manipulator: For the manipulator experiment, a single string was pulled by a mechanical testing machine (Instron 3345) at 300 mm min^{-1} until 200 mm under eight jamming conditions, corresponding to all possible permutations of active and inactive states for the three applied skins. To keep the motion in-plane for simplicity, Teflon was adhered to the bottom of the system and the manipulator rested on a fabric background. To stabilize the base, an acrylic cylinder was inserted into the foam tube such that approximately 2 cm of the skin closest to the base overlapped the acrylic. Video was captured from directly above the manipulator, and the manipulator tip was tracked by extracting the centroid of a piece of red tape placed on the end effector, using MATLAB's computer vision toolbox.

Supporting Information

Supporting Information is available from the Wiley Online Library or from the author.

Conflict of Interest

The authors declare no conflict of interest.

Author Contributions

D.S.S. and R.K.-B. conceived the idea. D.S.S., E.J.Y., and E.C.H. designed and built the hardware. D.S.S., M.C.Y., E.J.Y., and E.C.H. designed and performed the experiments. D.S.S., M.C.Y., and R.K.-B. analyzed the results. All authors contributed to, and agree with, the content of the final version of the manuscript.

Data Availability

The data that support the findings of this study are available from the corresponding author upon reasonable request.

[1] W. M. Kier, K. K. Smith, *Zool. J. Linn. Soc.* **1985**, *83*, 307.
[2] Y. Yekutieli, R. Sagiv-Zohar, R. Aharonov, Y. Engel, B. Hochner, T. Flash, *J. Neurophysiol.* **2005**, *94*, 1443.
[3] T. R. Clites, A. S. Arnold, N. M. Singh, E. Kline, H. Chen, C. Tugman, B. Billadeau, A. A. Biewener, H. M. Herr, *J. Exp. Biol.* **2019**, *222*, jeb198325.
[4] S. Kim, C. Laschi, B. Trimmer, *Trends Biotechnol.* **2013**, *31*, 287.
[5] M. Manti, V. Cacucciolo, M. Cianchetti, *IEEE Rob. Autom. Mag.* **2016**, *23*, 93.
[6] L. Blanc, A. Delchambre, P. Lambert, *Actuators* **2017**, *6*, 23.
[7] M. C. Yuen, R. A. Bilodeau, R. K. Kramer, *IEEE Rob. Autom. Lett.* **2016**, *1*, 708.
[8] W. Shan, S. Diller, A. Tutcuoglu, C. Majidi, *Smart Mater. Struct.* **2015**, *24*, 065001.
[9] A. Tonazzini, S. Mintchev, B. Schubert, B. Mazzolai, J. Shintake, D. Floreano, *Adv. Mater.* **2016**, *28*, 10142.
[10] A. Shiva, A. Stilli, Y. Noh, A. Faragasso, I. D. Falco, G. Gerboni, M. Cianchetti, A. Menciassi, K. Althoefer, H. A. Wurdemann, *IEEE Rob. Autom. Lett.* **2016**, *1*, 632.
[11] S. Diller, C. Majidi, S. H. Collins, A Lightweight, Low Power Electroadhesive Clutch and Spring for Exoskeleton Actuation. IEEE, New York **2016**, pp. 682–689.
[12] V. Ramachandran, J. Shintake, D. Floreano, *Adv. Mater. Technol.* **2019**, *4*, 1800313.
[13] E. Brown, N. Rodenberg, J. Amend, A. Mozeika, E. Steltz, M. R. Zakin, H. Lipson, H. M. Jaeger, *Proc. Natl. Acad. Sci.* **2010**, *107*, 18809.
[14] S. Narang Yashraj, J. Vlassak Joost, D. Howe Robert, *Adv. Funct. Mater.* **2018**, *28*, 1707136.
[15] M. Cianchetti, T. Ranzani, G. Gerboni, T. Nanayakkara, K. Althoefer, P. Dasgupta, A. Menciassi, *Soft Robotics* **2014**, *1*, 122.
[16] A. Jiang, T. Ranzani, G. Gerboni, L. Lekstutyte, K. Althoefer, P. Dasgupta, T. Nanayakkara, *Soft Robotics* **2014**, *1*, 192.
[17] S. Hauser, M. Robertson, A. Ijspeert, J. Paik, *IEEE Rob. Autom. Lett.* **2017**, *2*, 849.
[18] S. Chopra, M. T. Tolley, N. Gravish, *IEEE Robotics and Automation Letters* **2020**, *5*, 3975, conference Name: IEEE Robotics and Automation Letters.
[19] A. A. Stanley, K. Hata, A. M. Okamura, In *2016 IEEE International Conference on Robotics and Automation (ICRA)*, **2016**, pp. 2718–2724.
[20] Y. S. Narang, A. Degirmenci, J. J. Vlassak, R. D. Howe, *IEEE Rob. Autom. Lett.* **2018**, *3*, 688.
[21] N. Vasios, Y. Narang, B. Aktaş, R. Howe, K. Bertoldi, *Eur. J. Mech. A, Solids* **2019**, *75*, 322.
[22] R. P. Behringer, B. Chakraborty, *Rep. Prog. Phys.* **2018**, *82*, 012601.
[23] V. Wall, R. Deimel, O. Brock, In *2015 IEEE International Conference on Robotics and Automation (ICRA)*, **2015**, pp. 252–257.
[24] Y. J. Kim, S. Cheng, S. Kim, K. Iagnemma, *IEEE Trans. Rob.* **2013**, *29*, 1031.
[25] M. Langer, E. Amanov, J. Burgner-Kahrs, *Soft Robotics* **2018**, *5*, 291.
[26] J. Ou, L. Yao, D. Tauber, J. Steimle, R. Niiyama, H. Ishii, In *Proceedings of the 8th International Conference on Tangible, Embedded and Embodied Interaction.* ACM, **2014**, pp. 65–72.

**ADVANCED
SCIENCE NEWS**

www.advancedsciencenews.com

**ADVANCED
FUNCTIONAL
MATERIALS**

www.afm-journal.de

[27] I. Choi, N. Corson, L. Peiros, E. W. Hawkes, S. Keller, S. Follmer, *IEEE Rob. Autom. Lett.* **2018**, *3*, 450.

[28] W. H. Choi, S. Kim, D. Lee, D. Shin, *IEEE Rob. Autom. Lett.* **2019**, *4*, 2539.

[29] W. M. v. Rees, E. Vouga, L. Mahadevan, *Proc. Natl. Acad. Sci.* **2017**, 201709025.

[30] T. Mitsuda, In *2017 IEEE World Haptics Conference (WHC)*, **2017**, pp. 364–369.

[31] J. A. Fan, W.-H. Yeo, Y. Su, Y. Hattori, W. Lee, S.-Y. Jung, Y. Zhang, Z. Liu, H. Cheng, L. Falgout, M. Bajema, T. Coleman, D. Gregoire, R. J. Larsen, Y. Huang, J. A. Rogers, *Nat. Commun.* **2014**, *5*, 1.

[32] Y. J. Kim, S. Cheng, S. Kim, K. Iagnemma, In *2012 IEEE/RSJ International Conference on Intelligent Robots and Systems*, **2012**, pp. 4251–4256.

[33] D. T. Lee, B. J. Schachter, *Int. J. Comput. Inf. Sci.* **1980**, *9*, 219.

[34] S. Kawamura, K. Kanaoka, Y. Nakayama, J. Jeon, D. Fujimoto, In *2003 IEEE International Conference on Robotics and Automation (Cat. No.03CH37422)*, volume 1, **2003**, pp. 816–821.

[35] J. W. Booth, D. Shah, J. C. Case, E. L. White, M. C. Yuen, O. Cyr-Choiniere, R. Kramer-Bottiglio, *Sci. Rob.* **2018**, *3*, eaat1853.

[36] F. Daerden, D. Lefeber, *Eur. J. Mech. Environ. Eng.* **2002**, *47*, 11.

[37] S.-M. An, J. Ryu, M. Cho, K.-J. Cho, *Smart Mater. Struct.* **2012**, *21*, 055009.

[38] D. Chen, Q. Pei, *Chem. Rev.* **2017**, *117*, 11239.

[39] D. S. Shah, M. C. Yuen, L. G. Tilton, E. J. Yang, R. Kramer-Bottiglio, *IEEE Rob. Autom. Lett.* **2019**, *4*, 2204.

[40] A. Chortos, J. Liu, Z. Bao, *Nat. Mater.* **2016**, *15*, 937.

[41] Z. Huang, Y. Hao, Y. Li, H. Hu, C. Wang, A. Nomoto, T. Pan, Y. Gu, Y. Chen, T. Zhang, W. Li, Y. Lei, N. Kim, C. Wang, L. Zhang, J. W. Ward, A. Maralani, X. Li, M. F. Durstock, A. Pisano, Y. Lin, S. Xu, *Nat. Electron.* **2018**, *1*, 473.

[42] J. C. Yang, J. Mun, S. Y. Kwon, S. Park, Z. Bao, S. Park, *Adv. Mater.* **2019**, *31*, 1904765.

[43] P. Mittendorfer, G. Cheng, In *2012 IEEE/RSJ International Conference on Intelligent Robots and Systems*, **2012**, pp. 4505–4510.

[44] S. Y. Kim, R. Baines, J. Booth, N. Vasios, K. Bertoldi, R. Kramer-Bottiglio, *Nat. Commun.* **2019**, *10*, 3464.